Talanta 253 (2023) 123974

Contents lists available at ScienceDirect

Talanta

journal homepage: www.elsevier.com/locate/talanta

# Determination and localization of specific proteins in individual ARPE-19 cells by single cell and laser ablation ICP-MS using iridium nanoclusters as label

Paula Menero-Valdés [a], Ana Lores-Padín [a], Beatriz Fernández [a,*], C. Derrick Quarles Jr. [b], Montserrat García [c,d], Héctor González-Iglesias [e], Rosario Pereiro [a,**]

[a] Department of Physical and Analytical Chemistry, University of Oviedo, Julian Clavería 8, Oviedo, 33006, Spain
[b] Elemental Scientific, Inc., 7277 World Communications Drive, Omaha, NE, 68122, USA
[c] Instituto Oftalmológico Fernández-Vega, Avda. Dres. Fernández-Vega, 34, Oviedo, 33012, Spain
[d] Department of Cellular Morphology and Biology, Faculty of Medicine, Julian Clavería, Oviedo, 33006, Spain
[e] Department of Technology and Biotechnology of Dairy Products, Instituto de Productos Lácteos de Asturias, Consejo Superior de Investigaciones Científicas (IPLA-CSIC), Villaviciosa, Spain

ARTICLE INFO

*Keywords:*
Retinal pigment epithelial cells
Iridium nanoclusters
Metal-labelled immunoprobe
sc-ICP-MS
LA-ICP-MS
Biomaging

ABSTRACT

Single cell-inductively coupled plasma-mass spectrometry (sc-ICP-MS) and laser ablation (LA)-ICP-MS have been complementary employed to develop a comprehensive study of APOE and claudin-1 expression in ARPE-19 cells submitted to a glucose treatment (100 mM, 48 h) that induces oxidative stress conditions. Results were compared with control cells. The determination of the two proteins by ICP-MS was sequentially carried out using specific immunoprobes labelled with IrNCs that offer a huge amplification (1760 ± 90 atoms of Ir on average). A novel sample introduction system, the microFAST Single Cell set-up, was employed for sc-ICP-MS analysis. This introduction system resulted in a cellular transport efficiency of 85 ± 9% for ARPE-19 cells (91 ± 5% using a PtNPs standard). After the proper immunocytochemistry protocol with the specific IrNCs immunoprobes in cell suspensions (sc-ICP-MS), the mass of APOE and claudin-1 in individual ARPE-19 cells was obtained. Average detection limits per cell by sc-ICP-MS were 0.02 fg of APOE and 3 ag of claudin-1. The results of sample analyses obtained by sc-ICP-MS were validated with commercial ELISA kits. The distribution of both target proteins in individual cells (fixated in the chamber wall) was unveiled by LA-ICP-MS. The high amplification provided by the IrNCs immunoprobes allowed the identification of APOE and claudin-1 within individual ARPE-19 cells. High resolution images were obtained using a laser spot of 2 × 2 μm.

## 1. Introduction

Cell populations in all biological systems are well-known for their heterogeneous nature. Furthermore, genome, transcriptome, and proteome cell-to-cell variations can be the origin of different pathologies [1]. The quantitative analysis of individual cells in a target population is currently a critical research area in order to evaluate cellular variability. Among the options, particular attention should be paid to inductively coupled plasma - mass spectrometry (ICP-MS) due to its low limits of detection, wide dynamic range, low matrix effects and the possibility of multi-elemental and multi-isotopic analysis [2].

Traditionally, cellular samples have been analyzed by conventional nebulization ICP-MS after digestion of the cell, providing information of the whole population as an average (so, information regarding individual heterogeneity is lost). However, detection of single cell events can be achieved if the ICP-MS is operated in time-resolved analysis (TRA) mode, where acquisition parameters have been optimized (e.g., dwell time in the microsecond to low millisecond time scale) and cells are introduced into the plasma as highly diluted suspensions. The basis for single cell ICP-MS (sc-ICP-MS) was established by Li et al. [3]. Although sc-ICP-MS is an active research topic, its Achilles heel is still the transport efficiency (low transport efficiency equates to lost sample information) [4]. Numerous sample introduction systems have been explored to overcome this issue, such as employing low volume or total

* Corresponding author.
** Corresponding author.
*E-mail addresses:* fernandezbeatriz@uniovi.es (B. Fernández), mrpereiro@uniovi.es (R. Pereiro).

https://doi.org/10.1016/j.talanta.2022.123974
Received 28 July 2022; Received in revised form 13 September 2022; Accepted 25 September 2022
Available online 29 September 2022

consumption spray chambers, micro-nebulizers, heating the spray chamber, etc., but maximizing sample transport efficiency is still a challenge.

Over the last few years, sc-ICP-MS has been applied for the analysis of endogenous elements in individual cells to better understand their biological functions [5,6], to study the cellular internalization of metallic nanoparticles (NPs) [7–10], as well as to assess the uptake of metallodrugs [11–13]. Moreover, the use of metal-labelled antibodies allows the determination of specific biomolecules within the cells. Lanthanide chelates [14,15] or lanthanide-MAXPAR® [16,17] have been reported as labels for the determination of cellular biomarkers. However, only one to tens of detectable atoms are available per label in such cases. The availability of high amplification labels is crucial for the determination of low concentrated cellular biomolecules. In this vein, the use of NPs has been also proposed [18], although the relatively large size of common NPs (several tens of nm) can block the recognition sites of the antibodies. Recently, Lores-Padín et al. [19] proposed the use of gold nanocluster (AuNC) labelled antibodies for the determination of cytosolic proteins. AuNCs offer a higher amplification (466 Au atoms per immunoprobe) compared to chelates or MAXPAR® and have a small core diameter (less than 3 nm), minimizing possible steric hindrances.

sc-ICP-MS can be used for a high throughput cell-by-cell quantitative determination of target biomolecules within cell cultures, but the biomolecules' distribution inside each cell cannot be afforded. This can be overcomed by directly sampling the cells using laser ablation (LA) coupled to ICP-MS. LA-ICP-MS is a powerful tool for elemental and isotopic analysis, providing the ability to obtain high resolution images from biological tissue sections and cells [4,20]. Regarding the analysis of individual cells, one of the main drawbacks for bioimaging at subcellular level is the loss in sensitivity when reducing the spot size [21]. Previous works have been focused on the imaging of metallic NPs internalized by the cells [22,23]. Theiner et al. [24] have studied the distribution of Fe and P (intrinsically present in the cells) as well as Pt (exogenously added to the cells with a cisplatin treatment). The bioimaging of cellular structures employing metallic labels (e.g., Ir intercalators and mDOTA ligands loaded with different lanthanide ions) have been also reported [21,25]. However, works related to the spatial distribution of specific biomolecules at subcellular level are scarce. Van Acker et al. [26] employed Ho-DTPA and Tm-DTPA chelates to label membrane receptors [26] and Lores-Padín et al. [27] used AuNCs for labeling cytosolic proteins in cultured cells.

In this work, we present for the first time using sc-ICP-MS and LA-ICP-MS as complementary techniques to get a comprehensive study of target proteins in individual cells; determination of proteins was carried out by sc-ICP-MS and their localization at subcellular level was afforded by LA-ICP-MS. In order to achieve a significant amplification to detect proteins at low concentration levels in the cell, IrNCs-labelled immunoprobes (1760 Ir atoms on average per immunoprobe) were employed. AuNCs have been previously reported for the determination of proteins in individual cells [19,27]. However, IrNCs exhibit enhanced performances both in terms of the label size and the amplification provided: the reported AuNCs had an average size of 2.7 nm and the labelled immunoprobe consisted of 466 Au atoms, whereas IrNCs have an average size of 1.89 nm while the labelled immunoprobe have 1760 Ir atoms. Therefore, the use of the IrNCs label, which offers an amplification more than 3 times greater than the AuNCs, would allow the determination of proteins that are naturally present in the cells at a lower concentration level.

As a proof of concept, the sequential determination of two proteins (apolipoprotein E; APOE and claudin-1) in individual cells from the same *in vitro* model (human retinal pigment epithelial cells; ARPE-19) was pursued using sc-ICP-MS and LA-ICP-MS, both in cultured cells subjected to a pro-oxidative stress treatment with glucose (GL) and control (CT) cells without the treatment. The RPE is a pigmented monolayer of hexagonal cells responsible for the nourishment and adhesion of the neurosensory retina [28]. This neuroepithelium is constantly subjected to oxidative stress from multiple sources including high glucose levels (i.e., hyperglycemia) [29]. Hyperglycemia-induced oxidative stress contributes to the progression of eye diseases, such as diabetic retinopathy [30], causing glycation of proteins and affecting their regulatory mechanisms [31]. These alterations may affect the expression of APOE lipid transport protein [32] or the claudin-1 tight junction protein [33], modifying the normal function of the RPE and the increased risk of eye diseases onset. Thus, APOE and claudin-1 have been selected as a case study in ARPE-19 cells to demonstrate the importance of sc- and LA-ICP-MS as complementary techniques for biological studies. Sample preparation strategies with cells in suspension and fixation into the chamber wells were respectively optimized for sc- and LA-ICP-MS analysis. To corroborate the quantitative results obtained for APOE and claudin-1 by sc-ICP-MS in ARPE-19 cells, commercial ELISA kits were employed. Additionally, immunofluorescence with commercial Alexa fluorophores was utilized for verification of the protein distribution.

## 2. Experimental

Details related to the reagents employed for the synthesis and characterization of the IrNCs and IrNCs-immunoprobes [34], the culture and incubation of ARPE-19 cells, the immunocytochemistry (ICC) assays for the detection of target proteins by MS and fluorescence, the cellular preparation for sc-ICP-MS and LA-ICP-MS, as well as the ELISA analyses are collected at **Electronic Supplementary Material (ESM).** Furthermore, protocols for the synthesis and characterization of IrNCs and IrNCs-immunoprobes are also described at **ESM**.

### 2.1. Instrumentation

sc-ICP-MS measurements were performed with an ICP-MS 7900 series (Agilent) coupled to a microFAST Single Cell system (Elemental Scientific, Inc.). The sample introduction system includes an autosampler, a CytoNeb nebulizer, a CytoSpray chamber and a one-piece ICP-MS torch. sc-ICP-MS data processing was performed with SPCaL software [35]. LA-ICP-MS measurements were carried out with an ICP-MS 7900 series coupled to a ESL193 laser ablation system (Elemental Scientific Lasers) equipped with a TwoVol2 ablation chamber and a dual concentric injector (DCI) interface. LA-ICP-MS data processing was performed with Iolite (v4) software (Elemental Scientific Lasers). Statistical T-tests and data presentation (i.e., charts, histograms and cell event profiles) was also carried out using Microsoft Excel.

Cell counting was done with a Neubauer hemocytometer (Sigma-Aldrich) and an optical microscope (Inverted Microscope Leica DM IL LED, Leica Microsystems) with a 10-fold magnification lens. Spectrophotometric ELISA, cellular viability and ROS assays were measured with a microplate reader (Victor X5, PerkinElmer). Immunofluorescence measurements were carried out with a Leica DM6000B optical microscope equipped with epifluorescence (RGB filter) and a DFC 310 camera.

### 2.2. Experimental methods

#### 2.2.1. ARPE-19 cells culture and GL treatment

ARPE-19 cells for sc-ICP-MS measurements were cultured in T75 Corning® flasks in an incubator at 37 °C and 5% $CO_2$ with supplemented DMEMF12 medium for cellular growth. Once the cells were confluent, the medium was changed to supplemented hybridoma serum-free medium. For LA-ICP-MS, cells were cultured in Nunc™ Lab-Tek™ chambers. Before plating the cells, the chamber wells were treated with 2 μg $cm^{-2}$ poly-L-lysine and incubated 2 h at 37 °C to enhance adhesion of the cells to the well surface. Wells were washed with PBS (0.1 M, pH 7.4) twice before culturing the cells ($3{\cdot}10^4$ cells $well^{-1}$) in DMEMF12. This cellular density allows the cells to be separated in the chambers allowing for analysis of individual cells by LA-ICP-MS. Cell medium was changed to supplemented hybridoma serum-free medium 24 h after plating the

cells. After 24 h in hybridoma medium, cells were either non-treated (CT) or treated with glucose.

Concerning the optimization of the GL treatment, ARPE-19 cells were cultured in 96-well microplates ($3{\cdot}10^3$ cells well$^{-1}$) in supplemented DMEMF12 medium and after 24 h the medium was changed to hybridoma serum-free medium. After 24 h in such medium, different concentrations of glucose (0–100 mM) were added to the cells, which remained in a glucose enriched medium for 48 h. The viability of the GL-treated cells was studied with a CyQuant™ Direct cell proliferation assay. A microplate reader was employed for measuring fluorescence emission with the excitation/emission filters of 485 nm/535 nm. Additionally, the ROS production was evaluated after 48 h of treatment. For such purpose, the cells were treated with 10 μM $H_2$DCFDA and incubated 30 min at 37 °C and 5% $CO_2$. The fluorescence emission was measured with the microplate reader. Another sample of cells was treated with 5 mM AAPH during 1 h as a positive control.

For sc-ICP-MS analysis, cells were trypsinized with 0.25% (v/v) trypsin EDTA for 3 min in the incubator. DMEMF12 medium was added to neutralize trypsin activity and the cells were collected in a Falcon tube. Afterwards, cells were centrifuged to remove supernatant and re-suspended in PBS (0.1 M, pH 7.4). Cellular fixation was performed in Eppendorf tubes; $1.2{\cdot}10^6$ cells suspended in 250 μL of PBS were added to each tube, mixed with 250 μL of 4% (v/v) PFA and incubated 10 min at room temperature (RT). Then the liquid was removed with mild centrifugation (3 min, 100 g-force) and cells were re-dissolved in 250 μL of 4% PFA and incubated another 10 min at RT. Cells were centrifuged to remove PFA and washed once with PBS to remove damaged cells. After centrifuging to remove the supernatant, the cells were re-suspended in PBS at a $1{\cdot}10^6$ cells mL$^{-1}$ concentration (counted with a Neubauer chamber) and stored at 4 °C until further use. In the case of LA-ICP-MS analysis, cells in the chambers were washed twice with PBS, 4% PFA was added for cellular fixation and the cells were then incubated for 10 min at RT. Wells were washed 3 times with PBS and stored at 4 °C in PBS.

### 2.2.2. Immunoassays with IrNCs immunoprobes for detection of proteins by sc-ICP-MS and LA-ICP-MS

Immunoassays in suspension were performed using IrNCs immunoprobes in order to determine the proteins of interest in ARPE-19 cells by sc-ICP-MS. For such purpose, IrNCs:Anti-h-APOE or IrNCs:Anti-h-claudin-1 immunoprobes were independently employed with CT and GL-treated cells. For sc-ICP-MS measurements, fixated cell suspensions ($1{\cdot}10^6$ cells mL$^{-1}$) were centrifuged to remove the PBS and incubated with 0.1% (v/v) Triton X-100 to permeabilize the cellular membrane for 15 min at RT. Cells were centrifuged and washed with PBS once and then a blocking solution was added to the cells (2% (m/v) BSA and 10% (v/v) serum) and incubated for 30 min at RT. Cells were centrifuged and supernatant was discarded. The corresponding IrNCs immunoprobe was added to the cells at the desired Ab concentration (10 μg mL$^{-1}$ for Anti-h-APOE and 7 μg mL$^{-1}$ for Anti-h-claudin-1) and incubated at RT for 1 h. Then the cells were washed with PBS. Cells were re-suspended in PBS ($1{\cdot}10^6$ cells mL$^{-1}$) and stored at 4 °C.

The immunoassay for LA-ICP-MS measurements was directly performed into the chamber wells. PBS was carefully removed from the chambers and then 0.1% Triton X-100 was added to the wells for 30 min at RT to permeabilize the cellular membranes. Wells were washed with PBS and then a blocking solution was added to the wells. After incubating the blocking solution for 1 h (RT), the solution was removed and the corresponding IrNCs immunoprobe was added to the wells and incubated for 15 h at 4 °C. Wells were washed three times with PBS and stored in PBS at 4 °C.

### 2.2.3. Analysis of ARPE-19 cells by sc- ICP-MS and LA-ICP-MS

ARPE-19 cells subjected to the immunoassay protocol were measured by sc-ICP-MS within 8 h in all experiments. Cells were diluted in 50 mM Trizma® buffer for introducing them into the ICP-MS. Different cellular concentrations were studied, ranging from $5{\cdot}10^3$ to $1{\cdot}10^6$ cell mL$^{-1}$. Cell suspensions were introduced into the plasma with the microFAST Single Cell system using a 10 μL min$^{-1}$ flow rate. The ICP-MS was operated in TRA mode and $^{193}Ir^+$ and $^{56}Fe^+$ intensity signals ($^{193}Ir^+$ from IrNCs immunoprobes and $^{56}Fe^+$ as constituent element of the cells) were measured sequentially for 30 s per isotope. Experimental parameters are collected in Table 1.

For data treatment, SPCaL software was employed to discriminate the cell events from the background. Different filters were applied depending on the isotope measured; Poisson filter was employed for $^{56}Fe^+$, employing $\varepsilon = 0.5$ criteria to set the limit of criticality ($L_c$) and the event limit of detection ($L_d$), whereas a Gaussian filter was selected for $^{193}Ir^+$ distribution, employing 5σ criteria to set the $L_d$. At the optimized dwell time (0.1 ms), cellular events consist in several data points. SPCaL reconstructs the signal for every individual cell integrating the area under the peak for each cellular event. Next, the signal of $^{193}Ir^+$ per event was transformed into absolute mass of Ir. For such purpose, an external calibration using an Ir liquid standard was carried out and the following parameters were taken into account: transport efficiency, sample flow rate, dwell time, net intensity of the cellular event and the slope of the calibration curve [11,19]. Finally, a similar methodology to that previously reported [27] was followed to calculate the amount of protein (APOE and claudin-1) from the mass of Ir per cell. The number of Ir atoms per immunoprobe (1760 ± 90 atoms on average) as well as the molecular mass of each protein (23 kDa for claudin-1 and 34 kDa for APOE) were considered for calculations.

Two suspensions were analyzed to determine the transport efficiency of the experimental set-up for sc-ICP-MS: a commercial 46 nm PtNPs standard and a solution of fixated ARPE-19 cells ($10^5$ cells mL$^{-1}$; CT cells and non-subjected to the immunoassay protocol). Under the working conditions, the transport efficiency using the PtNPs standard was found to be 91 ± 5% within the same day (5 replicates). However, taking into account that ARPE-19 cells have a different nature (e.g., different size and robustness) than PtNPs and, so, they do not have to exhibit the same behavior within the introduction system, the cellular transport efficiency value employed for calculations in the detection of proteins in ARPE-19 cells was determined by analyzing cells. Transport efficiency was determined as the ratio of detected Fe events (detection of Fe represents the presence of a cell) over the expected events (determined by counting with a Neubauer chamber) that should be detected for a sample of fixated ARPE-19 cells. Transport efficiency was found to be 85 ± 9% across 5 same-day replicates.

For LA-ICP-MS analysis, the walls of the chambers and the PBS solution were removed just before the measurement. The bioimaging of

**Table 1**
Operating conditions for the analysis of ARPE-19 cells by sc-ICP-MS and LA-ICP-MS.

| sc-ICP-MS | | LA-ICP-MS | |
|---|---|---|---|
| **Acquisition mode** | Single particle | **Acquisition mode** | Time resolved |
| **Dwell time** | 0.1 ms | **Dwell time** | 0.1 s |
| **Make-up Ar flow (CytoSpray)** | 0.8 L min$^{-1}$ | **Make-up Ar flow (DCI)** | 0.8 L min$^{-1}$ |
| **Nebulizer Ar flow (CytoNeb)** | 0.25 L min$^{-1}$ | | |
| **Plasma Ar flow** | 15 L min$^{-1}$ | **Plasma Ar flow** | 15 L min$^{-1}$ |
| **Measured isotopes** | $^{193}Ir^+$,$^{56}Fe^+$ (ARPE-19) $^{195}Pt^+$ (PtNPs) | **Measured isotopes** | $^{193}Ir^+$ (ARPE-19) |
| **$H_2$flow - Collision cell** | 2.5 mL min$^{-1}$ ($^{56}Fe^+$) | **He flow - Ablation cell** | 0.8 L min$^{-1}$ |
| **Sample flow rate – microFAST Single Cell** | 10 μL min$^{-1}$ | **Laser spot** | 2 × 2 μm; square |
| **Acquisition time** | 30 s per isotope | **Frequency** | 80 Hz |
| | | **Scan speed** | 8 μm min$^{-1}$ |
| | | **Fluence** | 9 J cm$^{-2}$ |
| | | **Washout** | 100 ms |

the proteins in individual ARPE-19 cells was carried out by using the experimental conditions indicated in Table 1. In order to obtain high-resolution 2D-images for individual cells, multiple line scanning mode with a squared spot size of 2 μm was applied. A laser pulse frequency of 80 Hz and a fluence of 9 J $cm^{-2}$ ensured the quantitative ablation of cellular thickness. Data processing (2D-images of $^{193}Ir^{+}$ distribution in individual ARPE-19 cells, histograms and single line profiles) were performed with Iolite (v4) software. Thermal gradient was chosen as the scale for 2D-images and median filter was applied.

## 3. Results and discussion

### 3.1. Optimization of the glucose-induced oxidative stress treatment

To evaluate the optimum concentration of glucose to induce oxidative stress in ARPE-19 cells without causing substantial cell death, ARPE-19 cells were subjected to GL treatment with different concentrations (0, 5, 10, 30, 60 and 100 mM) for 48 h and the cell viability and cellular production of ROS were investigated. Experimental results showed that cells were not significantly affected (Fig. S1A), even at the highest GL concentration assayed (96% viability with 100 mM GL). The GL treatment increases the production of ROS in ARPE-19 cells with concentrations larger than 30 mM: as indicated in Fig. S1B, significant differences (T-test, $\alpha = 0.05$) as compared to the control in the production of ROS were observed for 30 mM (p value = 0.002), 60 mM (p value = 0.002) and 100 mM (p value = 0.01) of glucose. Although the average production of ROS increased with the GL concentration, not all the cells were equally affected, increasing the standard deviation associated with the fluorescence emission at higher GL concentrations. Note that the positive control (5 mM AAPH) exhibited an emission significantly higher than 100 mM of GL (2.15 *vs* 1.70-fold change in fluorescence emission) and a larger standard deviation value. Considering the experimental results, 100 mM was the GL concentration selected for ARPE-19 cells treatment to ensure the overproduction of ROS species without compromising the cellular proliferation.

### 3.2. Determination of proteins in individual ARPE-19 cells by sc-ICP-MS

#### 3.2.1. Optimization of the cell concentration

In this work, ARPE-19 cells were introduced into the ICP-MS employing the microFAST Single Cell system operating at 10 μL $min^{-1}$ and TRA mode was selected in the ICP-MS to detect single cell events (0.1 ms dwell time). The cell concentration in the suspension was optimized to have a sufficiently diluted solution to avoid multiple events but concentrated enough to obtain representative data in each analysis. For such purpose, a sample of fixated ARPE-19 cells (CT cells without IrNCs immunoprobe) was dissolved in Trizma® at different cellular concentrations (in the range of $5{\cdot}10^{3}$–$1{\cdot}10^{6}$ cells $mL^{-1}$) and $^{56}Fe^{+}$ intensity signal was detected by sc-ICP-MS. Fe is a constituent of the cells which was measured to determine the transport efficiency as well as to ensure the cellular integrity. It is possible to know the cellular loss through the sample introduction system by comparing the number of cells in the original suspension (cells were counted before measuring them) with the number of Fe events detected by sc-ICP-MS. In addition, if cells lost their integrity, intracellular Fe is dissolved in the suspension and $^{56}Fe^{+}$ background increases in the time-resolved profile obtained by sc-ICP-MS.

As it can be observed in Fig. 1, the number of detected cellular events (following $^{56}Fe^{+}$ intensity) increased linearly ($r^2 = 0.991$) from $5{\cdot}10^{3}$ to $2{\cdot}10^{5}$ cells $mL^{-1}$. However, at greater cellular concentrations, the number of detected events did not follow the same trend. Additionally, as shown in Fig. 1 (secondary Y axis), the transport efficiency and the signal-to-background ratio values were greater than 0.8 from $5{\cdot}10^{3}$ to $1{\cdot}10^{5}$ cells $mL^{-1}$. At higher cellular concentrations, both transport efficiency and signal-to-noise ratio decreases significantly. Such trends can be attributed to different causes. As the concentration of the cells in the nebulized solution increases, so does the probability of having multiple cells being detected at the same time. It can be seen in Fig. S2 that the $^{56}Fe^{+}$ intensity of the cellular events did not change when increasing the cell concentration from $2{\cdot}10^{4}$ to $1{\cdot}10^{5}$ cells $mL^{-1}$ (Figs. S2A and S2C, respectively). However, at $1{\cdot}10^{6}$ cells $mL^{-1}$ (Fig. S2E) there were several events with a larger $^{56}Fe^{+}$ intensity (10,000 counts), which can be attributed to two or more cells detected simultaneously. Moreover, at higher cell concentration, cellular disruption occurs to a larger extent: the $^{56}Fe^{+}$ background for $1{\cdot}10^{5}$ and $1{\cdot}10^{6}$ cells $mL^{-1}$ was $28 \pm 6$ and $590 \pm 60$ counts, respectively (Figs. S2D and S2F). Thus, the analysis of concentrated samples produces significant cell damage. This effect was also observed with the signal to background ratio; the intensity of the events does not depend on the cell dilution and, therefore, as ionic background increased at higher cell concentration, the ratio decreased.

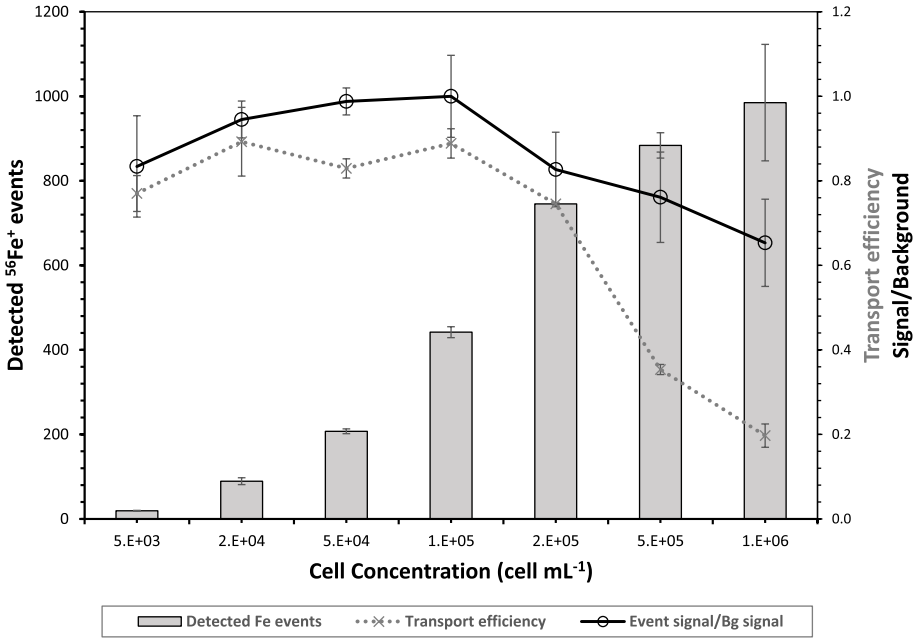


**Fig. 1.** Optimization of the ARPE-19 cell concentration in suspension for sc-ICP-MS analysis (CT cells without IrNCs immunoprobe). Grey bars indicate the number of Fe events detected ($^{56}Fe^{+}$ intensity signal) by sc-ICP-MS in 30 s; Grey dashed line indicates the transport efficiency (expressed as the ratio of number of detected cells over number of introduced cells); Black solid line indicates the normalized ratio of the average signal for the events over the signal for the background. Uncertainties indicate the standard deviation from the mean of three replicates.

The concentration selected for further sc-ICP-MS experiments was $1{\cdot}10^5$ cells $mL^{-1}$: the number of detected events was large enough to obtain representative data, the possibility of having multiple events was minimal and the signal-to-background ratio was maximized.

The cellular transport efficiency employed for calculations in the determination of proteins in ARPE-19 cells by sc-ICP-MS was determined with a cell suspension, showing an average value of 85 ± 9%. To the best of our knowledge this is the first time that the microFAST Single Cell system has been employed for the measurement of cells by sc-ICP-MS. Compared to previously described systems, the microFAST Single Cell allows short sampling periods as the transport efficiency obtained is significantly high. For example, cellular transport efficiencies in the range of 20–30% have been reported for the analysis of human ovarian carcinoma cells or red blood cells [11,36]. More recently, Lores-Padín et al. [19] set a transport efficiency of 8% for the analysis of HRPEsv cells using a high efficiency nebulizer and the Asperon® spray chamber.

### 3.2.2. *Optimization of the immunoassay using IrNCs as label*

The immunoassay protocols to label APOE and claudin-1 in ARPE-19 cells were optimized in terms of immunoprobe concentration (referred to as the Ab concentration) to ensure the total recognition of the proteins as well as the number of washing steps after treating the cells with the immunoprobe to avoid non-specific interactions. The protocols were independently carried out with the two immunoprobes: IrNCs:Anti-h-APOE and IrNCs:Anti-h-claudin-1. For the experiments, cells were diluted to $1{\cdot}10^5$ cells $mL^{-1}$, and $^{56}Fe^+$ and $^{193}Ir^+$ signals were sequentially detected by sc-ICP-MS in the same suspension. $^{56}Fe^+$ was measured to check the integrity of the cells and to confirm the number of cell events detected with $^{193}Ir^+$ (from the IrNCs immunoprobe). The data was fitted to a Poisson distribution in the case of $^{56}Fe^+$ and to a Gaussian filter in the case of $^{193}Ir^+$. The suitability of the filter depends on the background signal; higher counting rates work better with Gaussian filters, while Poisson filters work better with low background levels [35]. As it is described at **ESM** (see Fig. S3), if applying a Poisson filter to the $^{193}Ir^+$ signal, the $L_d$ was underestimated and the events coming from the free immunoprobes were detected as cellular events, overestimating the number of cells in the suspension. Nevertheless, when applying a Gaussian filter, events from IrNCs immunoprobe not specifically labelled to the cells were successfully discriminated. Thus, a Gaussian filter was applied to $^{193}Ir^+$, whereas the number of Fe events was calculated using Poisson filter.

Fig. 2 displays the experimental results obtained by sc-ICP-MS for the analysis of CT ARPE-19 cells labelled with IrNCs:Anti-h-APOE immunoprobe using different Ab concentrations (up to 40 μg $mL^{-1}$) and washing steps (1, 2 or 3). As it can be seen in Fig. S4, the ratio of detected events using $^{193}Ir^+$ intensity over detected events with $^{56}Fe^+$ intensity was close to one when employing immunoprobe concentrations from 5 to 40 μg $mL^{-1}$, independently of the number of washing steps. However, the ratio decreased with the lower Ab concentration (2 μg $mL^{-1}$), implying that it was not enough Ab to label all the proteins in ARPE-19 cells and some of them were not tagged. In Fig. 2, the mass of Ir (fg of Ir per cell) is shown for different immunoprobe concentrations (5–40 μg $mL^{-1}$ of Ab) using 1, 2 or 3 washing steps with PBS. As can be observed, the mass of Ir in the cells was approximately the same when adding 5 and 10 μg $mL^{-1}$ of Ab and it did not decrease with the washing steps. This means that the amount of Ab added to the cells was enough to label all the sought protein and the excess of Ab was successfully removed. However, the mass of Ir per cell when employing 20 and 40 μg $mL^{-1}$ of Ab and only one washing step was considerably higher and it decreased with the number of washing steps. This indicates an excess of Ab and, therefore, several washing steps were required to remove the immunoprobe not specifically bounded to APOE. In any case, when performing three washing steps, the mass of Ir per cell was approximately equal no matter the concentration of Ab, confirming that the possible excess of the immunoprobe can be efficiently removed with a proper washing procedure. It must be noted that the washing was manually performed with a micropipette and some cells can be lost in this procedure. For example, for the 10 μg $mL^{-1}$ concentration, 243, 205 and 96 cellular events were respectively detected for 1, 2 and 3 washing steps. Considering all the above, the selected concentration for IrNCs:Anti-h-APOE immunoprobe was 10 μg $mL^{-1}$ and 2 washing steps: this ensures an excess of Ab to recognize all the protein and an efficient washing to remove the excess of the immunoprobe without losing many cells. A similar approach was followed for the IrNCs:Anti-h-claudin-1 immunoprobe, being in this case 7 μg $mL^{-1}$ of Ab and 2 washing steps selected.

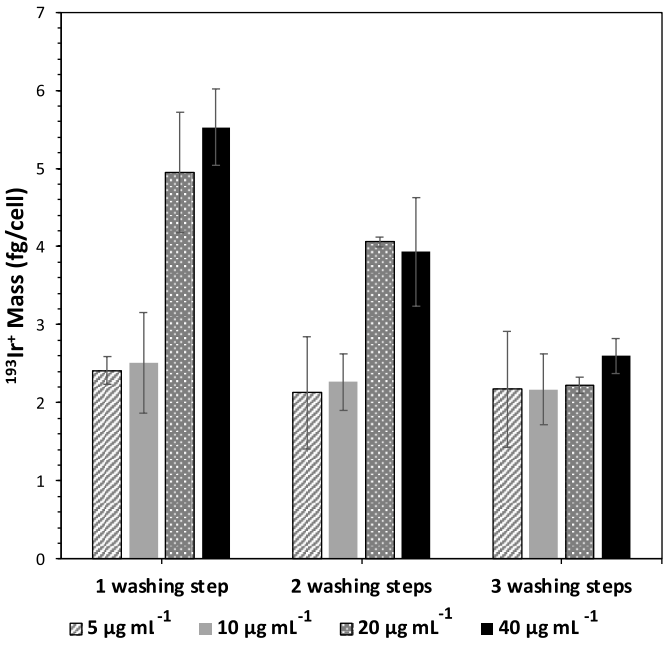


**Fig. 2.** Immunoassay optimization for the determination of APOE by sc-ICP-MS in CT ARPE-19 cells using IrNCs:Anti-h-APOE immunoprobe. Different Ab concentrations were evaluated in the immunoprobe as well as different washing steps with PBS (after incubation of the immunoprobe). The graph depicts the concentration of Ir per cell. Uncertainties represent the standard deviation from the mean of three replicates.

### 3.2.3. *Determination of APOE and claudin-1 by sc-ICP-MS*

APOE and claudin-1 were determined in CT and GL-treated ARPE-19 cells to study the possible variation of the protein expression after an induced oxidative stress treatment. Considering that the same label (IrNCs) was employed for both proteins, two batches of ARPE-19 cells (same passage) were used for the sequential determination of APOE and claudin-1 using IrNCs:Anti-h-APOE or IrNCs:Anti-h-claudin-1 immunoprobes, respectively. Data obtained by sc-ICP-MS were treated with SPCaL software and the intensity of $^{193}Ir^+$ was first transformed into mass of Ir per cell and subsequently, taking into account the immunoprobe amplification factor, into mass of protein per cell.

*3.2.3.1. Determination of APOE in CT and GL-treated ARPE-19 cells.* The effect of oxidative stress induced by glucose in the expression of APOE in ARPE-19 cells was studied in individual CT and GL-treated cells by sc-ICP-MS. As an example, Figs. S5A and S5B depict the time-resolved profiles obtained for $^{193}Ir^+$ for CT and GL-treated ARPE-19 cells, respectively. Furthermore, Table S1 contains the results obtained for five independent biological replicates of both conditions, each of them with three analytical replicates. As it can be seen, the number of detected Ir events was comparable to the number of detected Fe events in all cases, demonstrating that the IrNCs immunoprobe successfully labelled ARPE-19 cells. As it is collected in Table 2, taking into account

**Table 2**
Experimental results obtained for the determination of APOE and claudin-1 in ARPE-19 cells by sc-ICP-MS using IrNCs immunoprobe as label. Five biological replicates per condition were analyzed (CT and GL-treated) with three analytical replicates per biological sample.

| | APOE | | | claudin-1 | |
|---|---|---|---|---|---|
| Samples | fg APOE/cell | fg APOE/cell | Samples | ag claudin-1/cell | ag claudin-1/cell |
| **CT1** | 0.40 ± 0.05 | **0.38 ± 0.05** | **CT1** | 43 ± 5 | **42 ± 3** |
| **CT2** | 0.337 ± 0.003 | | **CT2** | 40.0 ± 0.6 | |
| **CT3** | 0.40 ± 0.05 | | **CT3** | 42 ± 4 | |
| **CT4** | 0.45 ± 0.06 | | **CT4** | 46 ± 5 | |
| **CT5** | 0.33 ± 0.06 | | **CT5** | 38 ± 1 | |
| **GL-treated 1** | 0.30 ± 0.01 | **0.28 ± 0.04** | **GL-treated 1** | 52 ± 4 | **63 ± 7** |
| **GL-treated 2** | 0.29 ± 0.03 | | **GL-treated 2** | 66 ± 5 | |
| **GL-treated 3** | 0.22 ± 0.01 | | **GL-treated 3** | 68 ± 14 | |
| **GL-treated 4** | 0.32 ± 0.02 | | **GL-treated 4** | 68 ± 12 | |
| **GL-treated 5** | 0.28 ± 0.03 | | **GL-treated 5** | 61 ± 5 | |

the average mass of APOE obtained for CT and GL-treated cells by sc-ICP-MS, the treatment of ARPE-19 cells with 100 mM GL for 48 h causes a downregulation of APOE synthesis: 0.38 ± 0.05 fg of APOE/cell for CT and 0.28 ± 0.04 fg of APOE/cell for GL-treated cells (1.4-fold change). Those results are found to be statistically different using T-test at 95% confidence (p value = 0.009). Concerning analytical performance of the method, the average APOE mass DL was 0.02 fg of APOE per cell, calculated by converting the $L_d$ of the applied Gaussian filter from counts of $^{193}Ir^+$ to fg of protein. Moreover, the uncertainty was found to be lower than 15% for both cellular groups.

To validate the results, a commercial ELISA kit was employed. A different batch of cells was cultured and either treated or non-treated with GL. After 48 h, cells were counted and suspended in a Tris-HCl buffer (to preserve proteins) and lysed by ultrasonication. The mass of APOE in the lysates was determined according to the specifications of the ELISA kit and referred to the number of cells previously determined with a Neubauer chamber. The average APOE mass determined by the ELISA kit (for three biological replicates and five analytical replicates) was found to be 0.38 ± 0.08 fg of APOE/cell for CT and 0.24 ± 0.08 fg of APOE/cell for GL-treated cells (1.6-fold change). Therefore, the results obtained by sc-ICP-MS were in agreement to those with the commercial kit. No significant differences were observed when comparing the results of sc-ICP-MS and the ELISA kit applying a T-test at 95% confidence interval to APOE mass for both the CT and GL-treated cells (p value = 0.99 for CT cells and 0.24 for GL-treated cells). The uncertainty obtained for the ELISA measurements was higher compared to that reported by sc-ICP-MS (20–30% with ELISA *versus* 15% with sc-ICP-MS).

In contrast to the ELISA kit, which only provides the average cellular protein mass in the cell population, sc-ICP-MS methodology allows for the determination of the mass of APOE in each cell within the cellular population. Fig. 3A shows the mass frequency histograms obtained (considering all the replicates for CT and GL-treated cells) representing the percentage of cells that contain a certain amount of the protein. As it can be seen in Table S1 where the minimum and maximum values obtained for the mass of APOE within each cell population have been included, the mass of APOE exhibited a huge variability from cell to cell, ranging for example from 0.001 to 3 fg of APOE/cell in the same cell suspension (CT1; R1). The histogram obtained for ARPE-19 cells (see Fig. 3A) shows that around 30% of the GL-treated cells were significantly affected by the hyperglycemic treatment inducing oxidative stress and the mass of APOE in such cells lied in between 0 and 0.05 fg/cell. Concerning CT cells, the mass of APOE for 82% of the cell population was within the interval 0.1–0.7 fg/cell, whereas only 61% of the GL-treated cell population lied within that range. At APOE masses above 0.7 fg/cell, both groups show a similar behavior. The same tendencies were observed for the histograms of each individual biological replicate, included in the ESM as Figs. S6A and S6B (CT and GL-treated cells, respectively). APOE is a RPE secreted protein, usually observed in the cytoplasm, responsible of lipid transport and its accumulation [37]. Alterations in the expression and localization of APOE have been related with the lipid-rich deposits observed under the basal lamina of the RPE

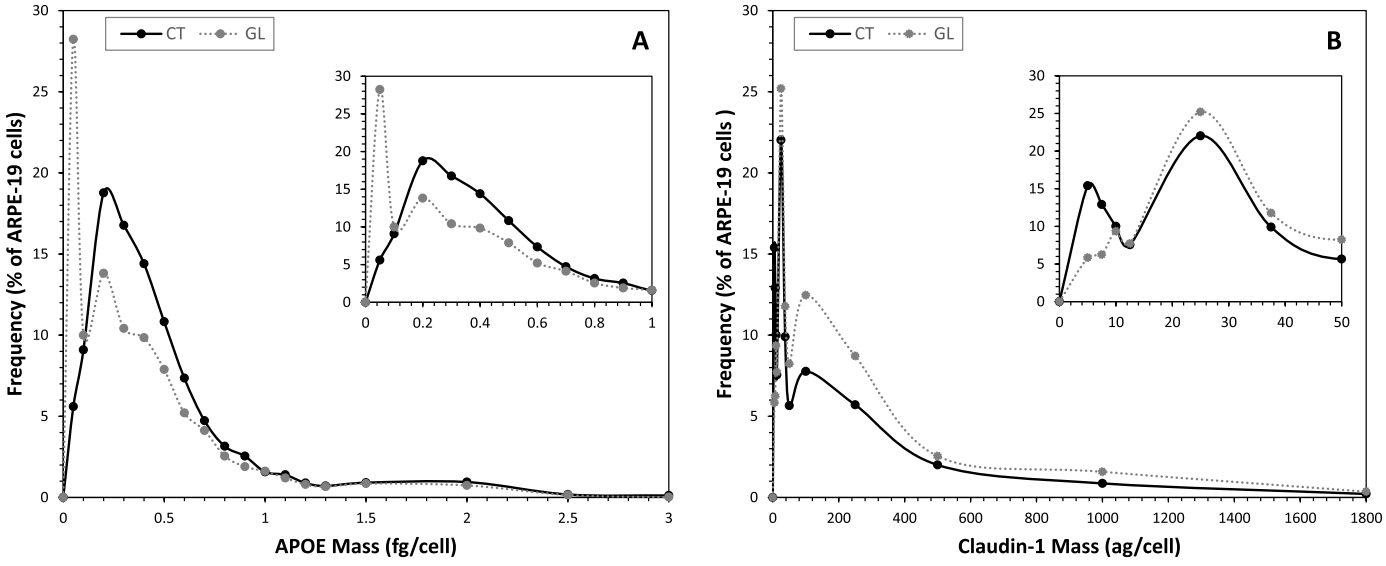


**Fig. 3.** Mass frequency histogram (in percentage) for APOE and claudin-1 in CT (black line) and glucose-treated (dotted grey line) ARPE-19 cells obtained by sc-ICP-MS using respectively Anti-h-APOE and Anti-h-claudin-1 immunoprobes. Both graphs are constructed with all the biological and analytical replicates measured. A) APOE; B) Claudin-1.

as a consequence of its progressive degeneration [38]. Previous studies showed that oxidant stress significantly reduced APOE at mRNA and protein levels [32], which seems to share common mechanism with high GL treatment [39]. The observed downregulation of APOE during oxidative stress conditions induced by glucose may be a regulatory mechanism to avoid an excessive APOE secretion [40]. However, according to our results, each ARPE-19 cell seems to respond differently considering that some cells induced APOE synthesis, and the majority inhibited it, highlighting the importance of determining the effect on each cell.

*3.2.3.2. Determination of claudin-1 in CT and GL-treated ARPE-19 cells.* The same methodology was applied to ARPE-19 cells labelled with the IrNCs:Anti-h-claudin-1 immunoprobe to determine claudin-1 in the cell population by sc-ICP-MS. Figs. S7A and S7B show the $^{193}Ir^{+}$ time-resolved profiles obtained for CT and GL-treated cells, respectively. Table 2 depicts the results obtained for the determination of claudin-1 mass in CT and GL ARPE-19 cells. In contrast to that observed for APOE, the GL treatment caused an overexpression of claudin-1 in ARPE-19 cells (1.5-fold change); the average claudin-1 mass was 42 ± 3 ag/cell for CT and 63 ± 7 ag/cell for GL-treated cells. Those results are statistically significantly different when applying a T-test at 95% confidence (p value = $4{\cdot}10^{-7}$). As reported for APOE, there is a huge disparity in the mass of claudin-1 among the same cell population (see the minimum and maximum values in Table S2). This fact can be graphically observed in Fig. 3B for the mass frequency histograms obtained for CT and GL-treated cell (average values taking into account all the biological and analytical replicates). Experimental results showed that 38% of the CT cell population had a claudin-1 mass between 5 and 10 ag/cell, whereas only 21% of GL cells lied within that range. GL treatment also increased the percentage of cells with a claudin-1 mass in the range of 50–500 ag/cell. Figs. S8A and S8B depict the mass frequency histograms for each individual biological replicate in CT and GL-treated cells, respectively.

The mass DL for claudin-1 by sc-ICP-MS was found to be as low as 3 ag of claudin-1 per cell, demonstrating that the great amplification provided by the IrNCs label allows to detect specific proteins in individual cells at very low concentration levels. Additionally, even with the high biological heterogeneity found for biological systems, there is excellent precision obtained for the analysis of five biological replicates of ARPE-19 cells submitted to immunocytochemistry with IrNCs immunoprobe by sc-ICP-MS; uncertainty obtained for the determination of claudin-1 mass ranged from 2 to 20%. Experimental results obtained by sc-ICP-MS were validated measuring the average mass of claudin-1 in cell lysates with a commercial ELISA kit. Claudin-1 mass was found to be 63 ± 10 ag/cell in CT and 83 ± 14 ag/cell in GL-treated cells (1.3-fold change), confirming the upregulation of claudin-1 after the GL treatment. Claudin-1 belongs to the family of claudins, which are important components of the tight junctions critical for mainlining the RPE integrity *in vivo* [41]. Oxidative stress induced by glucose affects the barrier function and the expression of tight junction proteins in the RPE [42], inducing claudin-1 synthesis as a compensatory mechanism to increase of tight junction sealing function [33], which is in agreement with our results. However, similarly to what was observed for APOE, a specific population of ARPE-19 cells showed higher levels of claudin-1 following GL treatment, which may be due to a specific response mechanism or a different cell stage, highlighting again the importance of analyzing each cell as an individual entity.

### 3.3. Bioimaging of proteins in individual ARPE-19 cells by LA-ICP-MS

Once the determination of APOE and claudin-1 was performed by sc-ICP-MS in a suspension of ARPE-19 cells, the study was completed by evaluating the localization of the target proteins in individual cells fixated to the chamber wells by LA-ICP-MS. In this case, cells were cultured in the chambers at low cellular density to make sure they were spaced out well to avoid cell to cell overlap (e.g., see Fig. S9). Spatial distribution of APOE and claudin-1 in individual cells (CT and GL-treated) was studied by monitoring the $^{193}Ir^{+}$ intensity signal from IrNCs immunoprobes (IrNCs:Anti-h-APOE or IrNCs:Anti-h-claudin-1, respectively). Square laser spots of 2 × 2 μm (Table 1) were employed and experimental conditions were optimized as a compromise between high spatial resolution and sensitivity. Laser fluence was set as low as possible that still resulted in the ablation of the whole cell volume. All ARPE-19 cells analyzed had a similar thickness and the same scan focus was adjusted for the whole imaging.

Fig. 4A and B shows the 2D-images obtained for $^{193}Ir^{+}$ signal (counts) indicating the distribution of APOE in individual CT and GL-treated ARPE-19 cells, respectively. The optical images of the ablated areas (taken with the laser camera prior to ablation) are shown in Fig. S9. As can be observed, the target protein was detected in individual cells by LA-ICP-MS following IrNCs label. It can be seen that APOE distribution within individual cells was not homogeneous. Additionally, $^{193}Ir^{+}$ intensity varied significantly from cell to cell; the scale bars of Fig. 4 were set as a compromise to identify APOE in the different cells of the ablated regions. Figs. S10A and S10B show amplifications of the 2D-images obtained by LA-ICP-MS for CT and GL-treated cells where each individual cell has the scale bar adjusted to its particular case. Thus, it is possible to identify the subcellular distribution of the protein and identify the regions where APOE was at higher or lower levels. For example, $^{193}Ir^{+}$ intensities for cell #3 in CT cells (Fig. S10A) or cell #1 in GL-treated cells (Fig. S10B) were significantly higher compared to intensities obtained for the other cells (150 *versus* 400 counts as maximum values in CT cells and 100 *versus* 300 counts in GL cells). Differences observed for $^{193}Ir^{+}$ signal between cells, both in CT and GL-treated, seem to indicate that the expression of APOE can significantly change from cell to cell (in agreement with results obtained by sc-ICP-MS). Thus, LA-ICP-MS confirms that the protein distribution also varies cell-to-cell within the same cell population.

A similar trend was found for claudin-1 in CT and GL-treated cells by LA-ICP-MS. Fig. 5 shows the 2D-images obtained for $^{193}Ir^{+}$ signal (i.e., claudin-1 distribution) in individual ARPE-19 cells using the IrNCs:Anti-h-claudin-1 immunoprobe. For CT and GL-treated cells, $^{193}Ir^{+}$ intensities exhibited a non-homogenous distribution within the individual cells (Fig. 5A and B, respectively). Comparing the intensity signals obtained for APOE and claudin-1, it can be seen that the lower content of claudin-1 compared to APOE (ag/cell *versus* fg/cell level) was also evident in 2D-images. Figs. S11A and S11B show amplifications of the

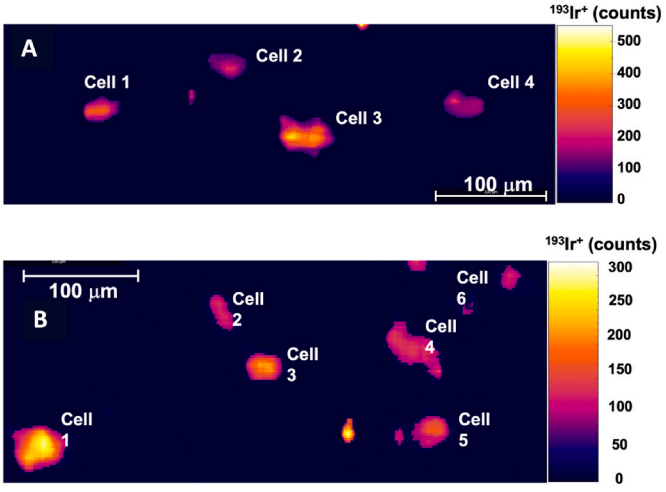


**Fig. 4.** Qualitative 2D-images obtained by LA-ICP-MS for $^{193}Ir^{+}$ signal (counts) using IrNCs:Anti-h-APOE immunoprobe in CT and GL-treated ARPE-19 cells. A) APOE distribution in CT cells, and B) APOE distribution in GL-treated cells.

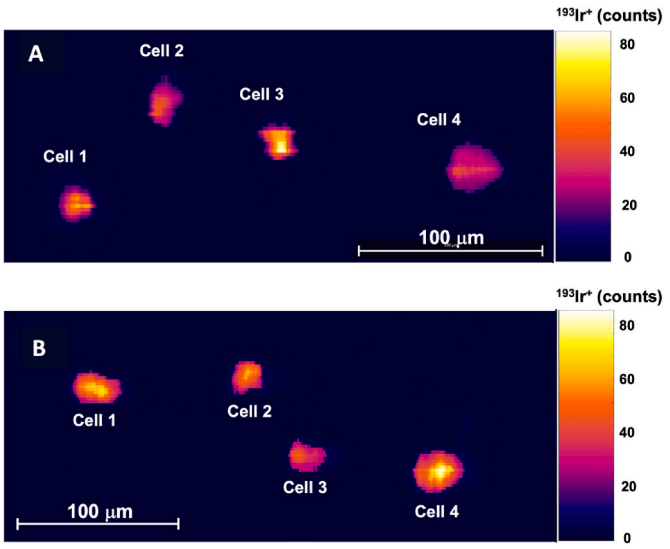


**Fig. 5.** Qualitative 2D-images obtained by LA-ICP-MS for $^{193}Ir^{+}$ signal (counts) using IrNCs:Anti-h-claudin-1 immunoprobe in CT and GLtreated ARPE-19 cells. A) Claudin-1 distribution in CT cells, and B) Claudin-1 distribution in GL-treated cells.

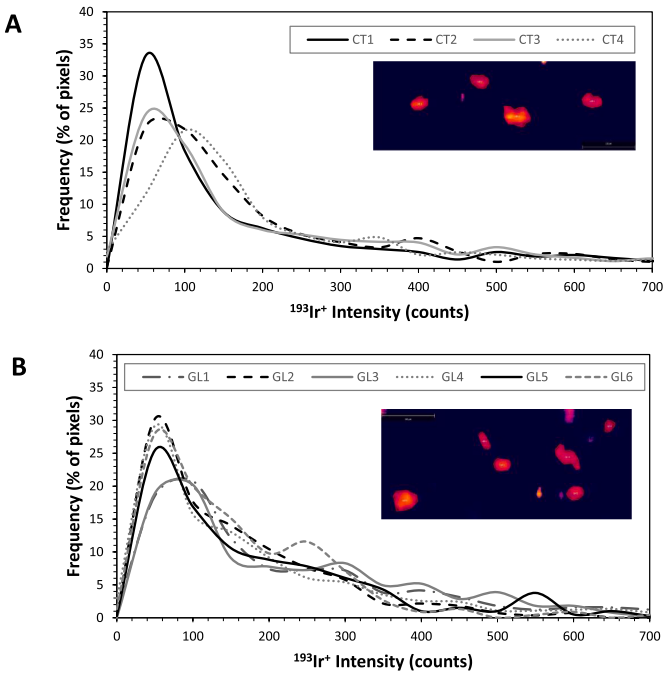


**Fig. 6.** Frequency histogram (in percentage of pixels) for APOE protein in ARPE-19 cells obtained by LA-ICP-MS analysis using Anti-h-APOE immunoprobe. The insets show the 2D-image obtained by LA-ICP-MS for the cells indicating the area of each individual cell (in red). A) CT cells; and B) GL-treated cells.

2D-images obtained for CT and GL-treated cells, respectively, with the scale bar adjusted to each individual cell; maximum values in the range of 35–100 counts were observed. The high amplification offered by the IrNCs label allowed for high resolution images for the protein localization within individual ARPE-19 cells. One of the main shortcomings when aiming to obtain subcellular resolution by LA-ICP-MS is the loss of sensitivity [21,25,43]. For example, Van Acker et al. [26] reported the use of DTPA chelates (containing just one detectable lanthanide atom per label) for the determination of membranous receptors in breast cancer cells by LA-ICP-MS, obtaining intensities for the lanthanides in the range of 0–20 counts. The concentration of those receptors in the cells was in the order of tens of fg/cell. Thus, the amplification provided by the IrNCs immunoprobe can be presented as a powerful performance, allowing the detection of proteins at low concentration levels in individual cells.

Iolite, v4 was used to construct 2D-images. On one hand, Fig. S12 depicts the single line profile obtained for $^{193}Ir^{+}$ intensity across individual cells for APOE; it is possible to see the variation of the protein distribution (in counts) along the cell diameter. As can be observed, the distribution of $^{193}Ir^{+}$ was not homogeneous across the cells, both in CT and GL-treated cells, indicating that APOE was more concentrated in certain cell regions. A similar trend was observed for claudin-1 (Fig. S13). The regions of interest (ROI) tool was used to access each individual cell, which resulted in a histogram, representing the frequency of pixels within the cell (that is directly related to the area of the cells) with a certain $^{193}Ir^{+}$ intensity (counts). As an example, the histograms corresponding to CT and GL-treated cells labelled with the IrNCs:Anti-h-APOE immunoprobe are shown in Fig. 6. All cells showed the same tendency; around 80% of the pixels within a cell have $^{193}Ir^{+}$ intensities below 400 counts, but there were some pixels within the cells with a greater intensity signal, up to 700 counts. Those pixels correspond to the areas within the cell where APOE was accumulated. In the case of claudin-1, the histograms depicted in Fig. S14 showed differences between the two cellular groups (CT and GL-treated). In the case of CT cells, around 55% of the pixels have an $^{193}Ir^{+}$ intensity below 20 counts, whereas only 30% of the pixels were below 20 counts in the case of GL-treated cells. Furthermore, a higher percentage of pixels with an $^{193}Ir^{+}$ intensity between 200 and 400 counts were observed for GL-treated compared to CT cells, indicating that claudin-1 was more heterogeneously distributed when cells were subjected to pro-oxidative stress conditions.

Finally, the distribution of APOE and claudin-1 observed by LA-ICP-MS was confirmed by conventional immunofluorescence. CT ARPE-19 cells fixated into chambers were subjected to an immunoassay protocol with fluorophore Alexa®594. In this case Anti-h-APOE and Anti-h-claudin-1 antibodies were independently added to the cells (without being previously bioconjugated to IrNCs) and then a secondary Ab labelled with fluorophore Alexa®594 was employed. As it can be seen in Fig. S15A, APOE was localized in the cellular cytoplasm [38], corroborating the spatial distribution obtained by LA-ICP-MS. Fig. S15B shows claudin-1 distribution unevenly throughout the cell, not observing its specific apicolateral localization [44] being expected since ARPE-19 cells were not confluent and their time in culture was lower than 5 days, being similar to the images obtained by LA-ICP-MS.

The combination of sc-ICP-MS and LA-ICP-MS allows a comprehensive study of the expression of endogenous proteins by cell populations submitted to different external stimuli. As a proof of concept, APOE and claudin-1 have been selected as the target proteins in ARPE-19 cells (under control and pro-oxidative stress conditions) due to their direct implication in eye related pathologies whose biological mechanisms are not currently fully understood. The same kind of sample (cells of the same line, subjected to equal external conditions) were analyzed with both techniques using a unique metal label (IrNCs). sc-ICP-MS measurements provide quantitative information regarding the concentration of APOE and claudin-1 in individual ARPE-19 cells. The data obtained include the protein concentration for each individual cell, but it is also possible to achieve the concentration range on the cellular population (between 150 and 400 cells were studied in each sc-ICP-MS analysis; ~7 min analysis time, including washing steps) and the maximum and minimum concentration in the cells suspension, providing valuable information of the sample heterogeneity. Additionally, frequency histograms (the distribution of the protein concentration among each sample of cells) can be obtained, allowing to better visualize the behavior of cell suspensions submitted to different treatments. In this particular case, differences between CT and GL-treated (100 mM, 48 h) ARPE-19 cells

were observed. On the other hand, for having a better understanding of the glucose treatment effect in APOE and claudin-1 concentration in ARPE-19 cells and its biological implication it is also important to study the intracellular localization of the proteins, as it can be altered due to oxidative stress [45,46]. Experimental results with LA-ICP-MS showed that APOE and claudin-1 exhibit a non-homogeneous distribution within cellular structures both for CT and GL-treated cells. Thus, not only a wide variability was observed for target proteins concentration in individual ARPE-19 cells, but also a non-homogeneous distribution of APOE and claudin-1 could be clearly identified within each cell. Differences in the proteins localization were not observed between CT and GL-treated ARPE-19 cells. The biological implications of the pro-oxidative stress treatment with glucose cannot be more deeply discussed since a higher number of samples should be evaluated, especially in the case of LA-ICP-MS (in this case, the analysis time for an imaging including 4 cells was ~120 min). However, the experimental results showed the potential of sc- and LA-ICP-MS as a tandem analytical tool to evaluate the effect of specific treatments in cells populations.

## 4. Conclusions

The evaluation of the effects induced by oxidative stress conditions in two proteins present in ARPE-cells was tackled with sc-ICP-MS and LA-ICP-MS. Specific antibodies labelled with IrNCs, which offer a huge amplification (1760 ± 90 atoms of Ir on average), were employed as immunoprobes for detection of APOE and claudin-1. Masses at the fg level for APOE and at the ag level for claudin-1 were determined by sc-ICP-MS in individual ARPE-19 cells. Concerning LA-ICP-MS, the high amplification provided by the IrNCs immunoprobes allowed the identification of APOE and claudin-1 in individual ARPE-19 cells. High resolution images were obtained, even for detection of claudin-1 that is present in ARPE-19 cells at the low ag/cell level.

This work shows the interest of the complementary use of sc-ICP-MS and LA-ICP-MS for comprehensive biological studies. LA-ICP-MS allows for the evaluation of the spatial distribution of target proteins in individual cells. However, it must be noted that the sample throughput (number of cells) is much higher by sc-ICP-MS. Finally, it is noteworthy to highlight the convenience of using immunoprobes containing a high number of detectable atoms, such as the antibodies labelled with IrNCs, in order to achieve low detection limits of the sought proteins.

## Credit author statement

Paula Menero-Valdés: Investigation, Methodology, Writing – original draft. Ana Lores-Padín: Validation, Review. Beatriz Fernández: Supervision, Conceptualization, Writing – review & editing. C. Derrick Quarles Jr.: Instrumental support. Montserrat García: Resources, Visualization. Héctor González-Iglesias: Conceptualization. Rosario Pereiro: Supervision, Funding acquisition, Review.

## Declaration of competing interest

The authors declare the following financial interests/personal relationships which may be considered as potential competing interests: Co-author C. Derrick Quarles Jr. works for Elemental Scientific which manufactures and sells the microFAST Single Cell system used in this work. The authors declare that the reported experimental results are not influenced by competing financial interests or personal relationships.

## Data availability

Data will be made available on request.

## Acknowledgements

This work was financially supported through projects PID2019-107838RB-I00/Agencia Estatal de Investigación (AEI)/10.13039/501100011033) in Spain and AYUD/2021/51289 - FICYT. P. Menero-Valdés acknowledges the FPU Grant with Ref. FPU19/00556 (Ministry of Education, Spain). Authors would like to acknowledge David Clases (University of Graz, Austria) for the support with SPCaL software and the technical support provided by Servicios Científico-Técnicos of the University of Oviedo.

## Appendix A. Supplementary data

Supplementary data to this article can be found online at https://doi.org/10.1016/j.talanta.2022.123974.

## References

[1] E. Shapiro, T. Biezuner, S. Linnarsson, Single-cell sequencing-based technologies will revolutionize whole-organism science, Nat. Rev. Genet. 14 (2013) 618–630, https://doi.org/10.1038/nrg3542.
[2] L. Mueller, H. Traub, N. Jakubowski, D. Drescher, V.I. Baranov, J. Kneipp, Trends in single-cell analysis by use of ICP-MS, Anal. Bioanal. Chem. 406 (2014) 6963–6977, https://doi.org/10.1007/s00216-014-8143-7.
[3] F. Li, D.W. Armstrong, R.S. Houk, Behavior of bacteria in the inductively coupled plasma: atomization and production of atomic ions for mass spectrometry, Anal. Chem. 77 (2005) 1407–1413, https://doi.org/10.1021/ac049188l.
[4] M. Resano, M. Aramendía, E. García-Ruiz, A. Bazo, E. Bolea-Fernandez, F. Vanhaecke, Living in a transient world: ICP-MS reinvented via time-resolved analysis for monitoring single events, Chem. Sci. (2022) 4436–4473, https://doi.org/10.1039/d1sc05452j.
[5] Z. Liu, A. Xue, H. Chen, S. Li, Quantitative determination of trace metals in single yeast cells by time-resolved ICP-MS using dissolved standards for calibration, Appl. Microbiol. Biotechnol. 103 (2019) 1475–1483, https://doi.org/10.1007/s00253-018-09587-w.
[6] K. Shigeta, G. Koellensperger, E. Rampler, H. Traub, L. Rottmann, U. Panne, A. Okino, N. Jakubowski, Sample introduction of single selenized yeast cells (Saccharomyces cerevisiae) by micro droplet generation into an ICP-sector field mass spectrometer for label-free detection of trace elements, J. Anal. At. Spectrom. 28 (2013) 637–645, https://doi.org/10.1039/c3ja30370e.
[7] L.N. Zheng, Y.B. Sang, R.P. Luo, B. Wang, F.T. Yi, M. Wang, W.Y. Feng, Determination of silver nanoparticles in single cells by microwell trapping and laser ablation ICP-MS determination, J. Anal. At. Spectrom. 34 (2019) 915–921, https://doi.org/10.1039/c8ja00438b.
[8] L. Rasmussen, H. Shi, W. Liu, K.B. Shannon, Quantification of silver nanoparticle interactions with yeast Saccharomyces cerevisiae studied using single-cell ICP-MS, Anal. Bioanal. Chem. 414 (2022) 3077–3086, https://doi.org/10.1007/s00216-022-03937-4.
[9] R.C. Merrifield, C. Stephan, J.R. Lead, Quantification of Au nanoparticle biouptake and distribution to freshwater algae using single cell - ICP-MS, Environ. Sci. Technol. 52 (2018) 2271–2277, https://doi.org/10.1021/acs.est.7b04968.
[10] Z. Chen, B. Chen, M. He, B. Hu, Droplet-splitting microchip online coupled with time-resolved ICPMS for analysis of released Fe and Pt in single cells treated with FePt nanoparticles, Anal. Chem. 92 (2020) 12208–12215, https://doi.org/10.1021/acs.analchem.0c01217.
[11] M. Corte Rodríguez, R. Álvarez-Fernández García, E. Blanco, J. Bettmer, M. Montes-Bayón, Quantitative evaluation of cisplatin uptake in sensitive and resistant individual cells by single-cell ICP-MS (SC-ICP-MS), Anal. Chem. 89 (2017) 11491–11497, https://doi.org/10.1021/acs.analchem.7b02746.
[12] L.N. Zheng, M. Wang, L.C. Zhao, B.Y. Sun, B. Wang, H.Q. Chen, Y.L. Zhao, Z. F. Chai, W.Y. Feng, Quantitative analysis of Gd@C82(OH)22 and cisplatin uptake in single cells by inductively coupled plasma mass spectrometry, Anal. Bioanal. Chem. 407 (2015) 2383–2391, https://doi.org/10.1007/s00216-014-8422-3.
[13] Y. Zhou, H. Li, H. Sun, Cytotoxicity of arsenic trioxide in single leukemia cells by time-resolved ICP-MS together with lanthanide tags, Chem. Commun. 53 (2017) 2970–2973, https://doi.org/10.1039/c7cc00143f.
[14] C. Liu, S. Lu, L. Yang, P. Chen, P. Bai, Q. Wang, Near-infrared neodymium tag for quantifying targeted biomarker and counting its host circulating tumor cells, Anal. Chem. 89 (2017) 9239–9246, https://doi.org/10.1021/acs.analchem.7b02016.
[15] Y. Liang, Q. Liu, Y. Zhou, S. Chen, L. Yang, M. Zhu, Q. Wang, Counting and recognizing single bacterial cells by a lanthanide-encoding inductively coupled plasma mass spectrometric approach, Anal. Chem. 91 (2019) 8341–8349, https://doi.org/10.1021/acs.analchem.9b01130.
[16] M. Corte-Rodríguez, E. Blanco-González, J. Bettmer, M. Montes-Bayón, Quantitative analysis of transferrin receptor 1 (TfR1) in individual breast cancer cells by means of labeled antibodies and elemental (ICP-MS) detection, Anal. Chem. 91 (2019) 15532–15538, https://doi.org/10.1021/acs.analchem.9b03438.
[17] A. Fernandez-Asensio, M. Corte-rodríguez, J. Bettmer, L.M. Sierra, M. Montes-Bayón, E. Blanco-González, Targeting HER2 protein in individual cells using ICP-MS detection and its potential as prognostic and predictive breast cancer biomarker, Talanta 235 (2021), 122773, https://doi.org/10.1016/j.talanta.2021.122773.
[18] R. Yuan, F. Ge, Y. Liang, Y. Zhou, L. Yang, Q. Wang, Viruslike element-tagged nanoparticle inductively coupled plasma mass spectrometry signal multiplier:

membrane biomarker mediated cell counting, Anal. Chem. 91 (2019) 4948–4952, https://doi.org/10.1021/acs.analchem.9b00749.
[19] A. Lores-Padín, E. Mavrakis, B. Fernández, M. García, H. González-Iglesias, R. Pereiro, S.A. Pergantis, Gold nanoclusters as elemental label for the sequential quantification of apolipoprotein E and metallothionein 2A in individual human cells of the retinal pigment epithelium using single cell-ICP-MS, Anal. Chim. Acta 1203 (2022), 339701, https://doi.org/10.1016/j.aca.2022.339701.
[20] M. Corte-Rodríguez, R. Álvarez-Fernández, P. García-Cancela, M. Montes-Bayón, J. Bettmer, Single cell ICP-MS using on line sample introduction systems: current developments and remaining challenges, TrAC, Trends Anal. Chem. 132 (2020), 116042, https://doi.org/10.1016/j.trac.2020.116042.
[21] A.J. Herrmann, S. Techritz, N. Jakubowski, A. Haase, A. Luch, U. Panne, L. Mueller, A simple metal staining procedure for identification and visualization of single cells by LA-ICP-MS, Analyst 142 (2017) 1703–1710, https://doi.org/10.1039/c6an02638a.
[22] J. Pisonero, D. Bouzas-Ramos, H. Traub, B. Cappella, C. Alvarez-Llamas, S. Richter, J.C. Mayo, J.M. Costa-Fernandez, N. Bordel, N. Jakubowski, Critical evaluation of fast and highly resolved elemental distribution in single cells using LA-ICP-SFMS, J. Anal. At. Spectrom. 34 (2019) 655–663, https://doi.org/10.1039/c8ja00096d.
[23] D. Drescher, C. Giesen, H. Traub, U. Panne, J. Kneipp, N. Jakubowski, Quantitative imaging of gold and silver nanoparticles in single eukaryotic cells by laser ablation ICP-MS, Anal. Chem. 84 (2012) 9684–9688, https://doi.org/10.1021/ac302639c.
[24] S. Theiner, A. Schweikert, S.J.M. Van Malderen, A. Schoeberl, S. Neumayer, P. Jilma, A. Peyrl, G. Koellensperger, Laser ablation-inductively coupled plasma time-of-flight mass spectrometry imaging of trace elements at the single-cell level for clinical practice, Anal. Chem. 91 (2019) 8207–8212, https://doi.org/10.1021/acs.analchem.9b00698.
[25] L. Mueller, A.J. Herrmann, S. Techritz, U. Panne, N. Jakubowski, Quantitative characterization of single cells by use of immunocytochemistry combined with multiplex LA-ICP-MS, Anal. Bioanal. Chem. 409 (2017) 3667–3676, https://doi.org/10.1007/s00216-017-0310-1.
[26] T. Van Acker, T. Buckle, S.J.M. Van Malderen, D.M. van Willigen, V. van Unen, F. W.B. van Leeuwen, F. Vanhaecke, High-resolution imaging and single-cell analysis via laser ablation-inductively coupled plasma-mass spectrometry for the determination of membranous receptor expression levels in breast cancer cell lines using receptor-specific hybrid tracers, Anal. Chim. Acta 1074 (2019) 43–53, https://doi.org/10.1016/j.aca.2019.04.064.
[27] A. Lores-Padín, B. Fernandez, M. Garcia, H. González-Iglesias, R. Pereiro, Real matrix-matched standards for quantitative bioimaging of cytosolic proteins in individual cells using metal nanoclusters as immunoprobes-label : a case study using laser ablation ICP-MS detection, Anal. Chim. Acta 1221 (2022), 340128, https://doi.org/10.1016/j.aca.2022.340128.
[28] O. Strauss, The retinal pigment epithelium in visual function, Physiol. Rev. 85 (2005) 845–881, https://doi.org/10.1152/physrev.00021.2004.
[29] T. Fiorentino, A. Prioletta, P. Zuo, F. Folli, Hyperglycemia-induced oxidative stress and its role in diabetes mellitus related cardiovascular diseases, Curr. Pharmaceut. Des. 19 (2013) 5695–5703, https://doi.org/10.2174/1381612811319320005.
[30] P.H. Scanlon, S.J. Aldington, I.M. Stratton, Epidemiological issues in diabetic retinopathy, Middle East Afr, J. Ophthalmol 20 (2013) 293–300, https://doi.org/10.4103/0974-9233.120007.
[31] H. Zheng, J. Wu, Z. Jin, L.-J. Yan, Protein modifications as manifestations of hyperglycemic glucotoxicity in diabetes and its complications, Biochem. Insights 9 (2016), https://doi.org/10.4137/bci.s36141. BCI.S36141.
[32] D.J. Espiritu, T. Mazzone, Oxidative stress regulates adipocyte apolipoprotein e and suppresses its expression in obesity, Diabetes 57 (2008) 2992–2998, https://doi.org/10.2337/db08-0592.
[33] M. Villarroel, M. García-Ramírez, L. Corraliza, C. Hernández, R. Simó, High glucose concentration leads to differential expression of tight junction proteins in human retinal pigment epithelial cells, Endocrinol. Nutr. 56 (2009) 53–58, https://doi.org/10.1016/S1575-0922(09)70552-2.
[34] P. Menero-Valdés, A. Lores-Padín, B. Fernández, H. González-Iglesias, R. Pereiro, Iridium nanoclusters as high sensitive-tunable elemental labels for immunoassays: determination of IgE and APOE in aqueous humor by inductively coupled plasma-mass spectrometry, Talanta 244 (2022), 123424, https://doi.org/10.1016/j.talanta.2022.123424.
[35] T.E. Lockwood, R. Gonzalez De Vega, D. Clases, An interactive Python-based data processing platform for single particle and single cell ICP-MS, J. Anal. At. Spectrom. 36 (2021) 2536–2544, https://doi.org/10.1039/d1ja00297j.
[36] Y. Cao, J. Feng, L. Tang, C. Yu, G. Mo, B. Deng, A highly efficient introduction system for single cell- ICP-MS and its application to detection of copper in single human red blood cells, Talanta 206 (2020), 120174, https://doi.org/10.1016/j.talanta.2019.120174.
[37] A.A. Bergen, S. Arya, C. Koster, M.G. Pilgrim, D. Wiatrek-Moumoulidis, P.J. van der Spek, S.M. Hauck, C.J.F. Boon, E. Emri, A.J. Stewart, I. Lengyel, On the origin of proteins in human drusen: the meet, greet and stick hypothesis, Prog. Retin. Eye Res. 70 (2019) 55–84, https://doi.org/10.1016/j.preteyeres.2018.12.003.
[38] M.G. Pilgrim, I. Lengyel, A. Lanzirotti, M. Newville, S. Fearn, E. Emri, J.C. Knowles, J.D. Messinger, R.W. Read, C. Guidry, C.A. Curcio, Subretinal pigment epithelial deposition of drusen components including hydroxyapatite in a primary cell culture model, Investig. Ophthalmol. Vis. Sci. 58 (2017) 708–719, https://doi.org/10.1167/iovs.16-21060.
[39] Y. Zhang, X. Xi, Y. Mei, X. Zhao, L. Zhou, M. Ma, S. Liu, X. Zha, Y. Yang, High-glucose induces retinal pigment epithelium mitochondrial pathways of apoptosis and inhibits mitophagy by regulating ROS/PINK1/Parkin signal pathway, Biomed. Pharmacother. 111 (2019) 1315–1325, https://doi.org/10.1016/j.biopha.2019.01.034.
[40] A. Saadane, A. Petrov, N. Mast, N. El-Darzi, T. Dao, A. Alnemri, Y. Song, J. L. Dunaief, I.A. Pikuleva, Mechanisms that minimize retinal impact of apolipoprotein E absence, J. Lipid Res. 59 (2018) 2368–2382, https://doi.org/10.1194/jlr.M090043.
[41] A. Gonçalves, A.F. Ambrósio, R. Fernandes, Regulation of claudins in blood-tissue barriers under physiological and pathological states, Tissue Barriers 1 (2013), e24782, https://doi.org/10.4161/tisb.24782.
[42] M. Villarroel, M. García-Ramírez, L. Corraliza, C. Hernández, R. Simó, Effects of high glucose concentration on the barrier function and the expression of tight junction proteins in human retinal pigment epithelial cells, Exp. Eye Res. 89 (2009) 913–920, https://doi.org/10.1016/j.exer.2009.07.017.
[43] C. Giesen, L. Waentig, T. Mairinger, D. Drescher, J. Kneipp, P.H. Roos, U. Panne, N. Jakubowski, Iodine as an elemental marker for imaging of single cells and tissue sections by laser ablation inductively coupled plasma mass spectrometry, J. Anal. At. Spectrom. 26 (2011) 2160–2165, https://doi.org/10.1039/c1ja10227c.
[44] F. Farjood, E. Vargis, Physical disruption of cell–cell contact induces VEGF expression in RPE cells, Mol. Vis. 23 (2017) 431–446.
[45] G. Filomeni, D. De Zio, F. Cecconi, Oxidative stress and autophagy: the clash between damage and metabolic needs, Cell Death Differ. 22 (2015) 377–388, https://doi.org/10.1038/cdd.2014.150.
[46] C. Vogel, G.M. Silva, E.M. Marcotte, Protein expression regulation under oxidative stress, Mol. Cell. Proteomics 10 (2011) 1–12, https://doi.org/10.1074/mcp.M111.009217.